THE ASTROPHYSICAL JOURNAL LETTERS, 727:L20 (5PP), 2011 JANUARY 20
Preprint typeset using LaTeX style emulateapj v. 11/26/04

ON THE DENSITY DISTRIBUTION IN STAR-FORMING INTERSTELLAR CLOUDS

ALEXEI G. KRITSUK,[1] MICHAEL L. NORMAN,[1,2] AND RICK WAGNER[2]
[1]Physics Department and Center for Astrophysics & Space Sciences, University of California, San Diego, 9500 Gilman Drive, La Jolla, CA 92093-0424, USA
[2]San Diego Supercomputer Center, University of California, San Diego, 10100 Hopkins Drive, La Jolla, CA 92093-0505, USA
Received 2010 July 16; accepted 2010 December 10; published 2010 December 29

ABSTRACT

We use deep adaptive mesh refinement simulations of isothermal self-gravitating supersonic turbulence to study the imprints of gravity on the mass density distribution in molecular clouds. The simulations show that the density distribution in self-gravitating clouds develops an *extended* power-law tail at high densities on top of the usual lognormal. We associate the origin of the tail with self-similar collapse solutions and predict the power index values in the range from $-7/4$ to $-3/2$ that agree with both simulations and observations of star-forming molecular clouds.

Subject headings: ISM: structure — methods: numerical — stars: formation — turbulence

1. INTRODUCTION

The probability density function (PDF) of the mass density in non-self-gravitating isothermal supersonic turbulence is believed to be lognormal (Vazquez-Semadeni 1994; Passot & Vázquez-Semadeni 1998; Padoan & Nordlund 1999; Kritsuk et al. 2007). Some hints of power-law tails, however, have been noticed in numerical simulations of the self-gravitating turbulent interstellar medium (ISM; e.g., Scalo et al. 1998; Klessen 2000; Dib & Burkert 2005; Slyz et al. 2005; Vázquez-Semadeni et al. 2008; Federrath et al. 2008; Collins et al. 2010). More recently similar tails were also found in high dynamic range observations of star-forming molecular clouds (Kainulainen et al. 2009; Lombardi et al. 2010). While it is understood that the density PDF holds the key to phenomenology of star formation (e.g., Padoan & Nordlund 2002; Krumholz & McKee 2005; Hennebelle & Chabrier 2008; Cho & Kim 2011), the origin of the power-law tail in self-gravitating supersonic turbulence still awaits a credible explanation. A related question pertains to the power index value for the tail.

Slyz et al. (2005) find a slope of −1.5 in non-magnetic kpc-scale interstellar turbulence simulations, while Collins et al. (2010) measured −1.6 in isothermal adaptive mesh refinement (AMR) MHD simulations of supersonic molecular cloud turbulence in a 10 pc box. Is there a universal power index value that applies to self-gravitating isothermal turbulence? What determines the slope? To address these questions, we analyze a deep AMR simulation with a linear dynamic range of 5×10^5 that follows the star formation process from turbulent initial conditions on a scale of a few pc down to a few AU.

We describe the simulation detail in the following section, while Section 3 presents the analysis of the density distribution and provides testable predictions for the power index values. Section 4 discusses the limitations of the model and effects of the magnetic field on the density PDF. The final section outlines conclusions.

2. NUMERICAL EXPERIMENT

Our star formation simulation was performed with the ENZO code for cosmology and astrophysics (O'Shea et al. 2005) and discussed earlier in Padoan et al. (2005). We solve the hydrodynamic equations, including self-gravity and a large-scale random force to drive the turbulence. We also adopt an isothermal equation of state and periodic boundary conditions. In this simulation, AMR is automatically carried out in collapsing regions in order to properly resolve the Jeans length (Truelove et al. 1997). We use root grid of 512^3 cells and five AMR levels with a refinement factor of four. The computational box has a size $L = 5$ pc, and the gravitational collapse of dense protostellar cores is resolved down to the scale of 2 AU. The temperature is uniform, $T = 10$ K, and the sound speed is constant, $c_s = 0.2$ km s^{-1}. The mean density $n_0(H_2) = 500$ cm^{-3} and the rms flow velocity of 1.1km s^{-1}, typical of molecular clouds on scales of ~ 5 pc, correspond to sonic Mach number $M_s \approx 6$. The free-fall time

$$t_{\rm ff} \equiv \sqrt{\frac{3\pi}{32G\rho}} \approx 1.6\ {\rm Myr}, \tag{1}$$

the dynamical time

$$t_{\rm dyn} \equiv \frac{L}{2M_s c_s} \approx 2.3\ {\rm Myr}, \tag{2}$$

and the virial parameter for this model

$$\alpha \equiv \frac{5\sigma_{3D}^2 R}{3GM} \approx 0.25, \tag{3}$$

correspond to a $3.4\times10^3\ M_\odot$ molecular cloud prone to collapse on its free-fall timescale. Indeed, the dendrogram analysis applied to a snapshot from a larger 1024^3 simulation (Kritsuk et al. 2007) resembling the initial conditions adopted here, indicated the presence of gravitationally bound objects on essentially all scales within the computational domain (Rosolowsky et al. 2008).

We began the simulation as a uniform grid turbulence model by stirring the gas in the computational domain for $4.8t_{\rm dyn}$ with a large-scale random force that includes 40% dilatational and 60% solenoidal power and then, at $t = 0$, turned the forcing off to continue the simulation with AMR and self-gravity for about $0.29t_{\rm dyn} \approx 0.43t_{\rm ff}$.

3. EFFECTS OF SELF-GRAVITY

Figure 1 shows the density distributions in this simulation. The red line corresponds to the initial condition at $t = 0$, when we turn on self-gravity. The density PDF at this time can be perfectly represented by a lognormal distribution (Kritsuk et al. 2007). Once gravity starts to operate, a power-law tail develops at the high end of the distribution. After

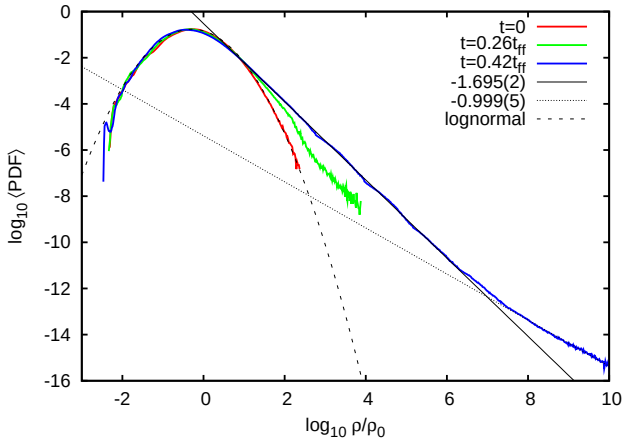

FIG. 1.— Probability distribution functions for the mass density from an AMR simulation of self-gravitating isothermal turbulence. The red line shows the initial conditions corresponding to a driven, statistically steady Mach 6 turbulence with no self-gravity. The green line shows the PDF for self-gravitating gas after $0.26t_{\rm ff}$ of evolution from the initial conditions. The effective linear dynamic range of the simulation at this instance in time is 2048. The blue line shows a time-average PDF at $0.42\pm0.01t_{\rm ff}$; time averaging helps to reduce the statistical noise at high densities. The dynamic range is 5×10^5. The initial conditions can be approximated by a lognormal distribution (dashed line). A power law with a slope of -1.695 ± 0.002 (solid line) provides the best fit to the high-density tail at $\rho/\rho_0\in[10,10^7]$. The break in the power index at $\rho/\rho_0\sim10^7$ marks a transition to rotationally supported cores (slope –1, dotted line).

$0.26t_{\rm ff}$, when the creation of first-level AMR subgrids is triggered by the first collapsing objects, the density distribution no longer remains lognormal. As the collapse of these first objects proceeds, followed by further grid refinement, an extended power-law tail emerges with a slope of about −1.7. The tail departs from the initial lognormal distribution already at $\rho/\rho_0\sim10$ and continues straight for nearly 10 dex in probability and more than 6 dex in density. As the simulation progresses, the slope continues to evolve slowly toward shallower values. The power index at the end of the simulation is −1.67. An even shallower tail at very high densities, $\rho/\rho_0>10^7$, develops as an indication of mass pile-up due to an additional support against gravity that comes from the conservation of angular momentum.[1] The power index for this centrifugally supported part of the density distribution is very close to −1.0. The fact that the power law breaks at a density slightly in excess of $10^7\rho_0$ may indicate the minimum grid resolution requirement for convergence in star formation simulations with sink particles (roughly 32,000 for this set of parameters), but the main focus of this Letter is on the origin of the extended power law at densities below $10^7\rho_0$. Why does it cover over six orders of magnitude in mass density without a tiny bit of slope change? What fundamental physics is involved?

Let us first recall that supersonic turbulence is a multi-scale phenomenon shaping the structure of the mass distribution in molecular clouds (e.g., von Weizsäcker 1951; Biglari & Diamond 1988; Kritsuk et al. 2006). At Mach numbers, $M_s>3$, the turbulence creates a "fractal" density distribution with the mass dimension of $D_{\rm m}\sim2.3$ (Elmegreen & Falgarone 1996; Kritsuk et al. 2007). Since this mass dimension is larger than the critical value for gravitational instability, $D_{\rm m}>D_{\rm crit}=2$, these highly inhomogeneous systems are still subject to gravitational collapse (Perdang 1990).

The extent of the power law we obtain in the deep AMR simulation hints at the tail origin in the hierarchical nature of gravitational collapse of dense structures in molecular clouds. Let us take a look at the very bottom of the hierarchy, where AMR resolves collapsed protostellar cores. We used density fields for approximately cubic subvolumes centered on several selected dense cores to obtain the PDFs in the immediate vicinity of these objects. The linear size of these subvolumes is of order 0.005 pc. Figure 2 offers three example PDFs and volumetric rendering of the corresponding cores. Stretches of the power-law distributions are clearly present in all three cases, although the slopes vary from as shallow as −1.25 to as steep as −1.75.[2] When the contributions from individual cores combine to form the density PDF for the whole computational domain, by some magic the resulting slope appears to be the same as that from the collapsing larger-scale structures characterized by a lower density, $\rho/\rho_0\in[10^2,10^5]$.

The easiest way to solve this puzzle is to assume that a self-similar collapse solution would act as a strong attractor determining the form of the density PDF in hierarchical, turbulent, self-gravitating molecular clouds. There is a large inventory of (semi-)analytical solutions for the collapse of spherically symmetric isothermal configurations to choose from. Whitworth & Summers (1985) arranged these similarity solutions into a banded two-dimensional continuum embracing the limiting cases of *fast* (Larson 1969; Penston 1969, hereafter LP) and *slow* (Shu 1977) collapse and their generalization by Hunter (1977). While this family of solutions describes gravitational condensation starting from a diverse set of idealized initial conditions, they have two important features in common. First, during the early stages of the evolution preceding the formation of a singularity at the center, all of them develop a $\rho\sim r^{-2}$ density profile.[3] Second, at late stages an expansion wave (EW) forms and propagates from the central singularity through the accreting material leaving behind a self-similar distribution with $\rho\sim r^{-3/2}$ at $r\to0$.

It can be readily shown that the mass density PDF for a spherically symmetric configuration with a $\rho=\rho_0(r/r_0)^{-n}$ density profile is a power law

$$dV=\frac{4}{3}\pi r_0^3\,d\left[\left(\frac{\rho}{\rho_0}\right)^{-3/n}\right]\propto d\left(\rho^m\right) \qquad (4)$$

with an index $m=-3/n$. Thus, formally, the similarity solutions generate power-law PDFs with a slope $m_{\rm LP}=-3/2$ corresponding to the r^{-2} profile during the early collapse stages and with a combination of slopes $m_{\rm LP}=-3/2$ (r^{-2} profile at lower densities) and $m_{\rm EW}=-2$ ($r^{-3/2}$ profile at higher densities) after the singularity has formed at the center. If the spherical symmetry is broken, for instance due to the presence of rotation, the situation becomes substantially more involved and hardly tractable analytically. Whitworth et al. (1996) suggest that a weak inward propagating compression wave that triggers the formation of the singularity would converge incoherently on the center and interfere with any reflected EW.

[1] It may partly be also due to our enforced limit on the number of allowed refinement levels (five levels maximum), which eventually violates the Truelove et al. (1997) numerical stability condition.

[2] Note that the rotation-induced pile-ups at highest densities are only visible in the two distributions that continue beyond $\rho/\rho_0=10^{10}$, while the third case shows only a hint of the pile-up at $\rho/\rho_0>10^7$. The first two cores have already developed relatively thin centrifugally supported disks, as can be seen in the renderings that show both face-on and edge-on views of the disks. The third core displays a rather modest flattening in the edge-on projection, indicating a weak rotation.

[3] The Shu (1977) singular isothermal sphere (SIS) solution represents a hydrostatic $\rho\sim r^{-2}$ configuration from the outset.

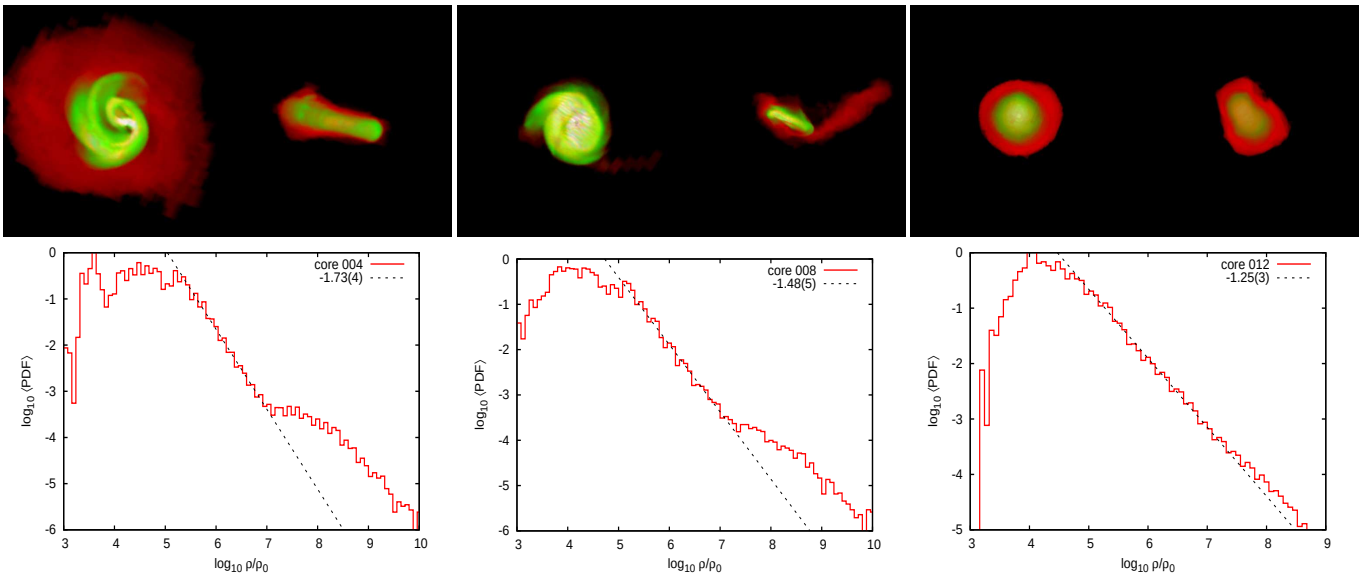

FIG. 2.— Volumetric rendering (top three panels) and PDFs (bottom) of the mass density for a sample of dense cores from the AMR simulation at $t = 0.42t_{\rm ff}$. The data represent $\sim 350^3$ extractions at the highest grid resolution achieved in the simulation (2 AU). The maximum densities are $\rho_{\rm max}/\rho_0 = 8.5\times10^{10}$, 3.2×10^{10}, and 6.0×10^{8} for the cores from left to right, respectively.

The interference would then cause a significant degradation in the density profile at small radii. We believe this lowers expectations for the pure EW solution in realistic situations. However, the r^{-2} density profile and the corresponding slope of the density PDF $m_{\rm LP} = -3/2$ could potentially be preserved if an equilibrium singular disk with a flat rotation curve would form at the center (Norman et al. 1980; Toomre 1982; Hayashi et al. 1982). Nevertheless, the disks formed in our simulation (Figure 2) typically show steeper density profiles ($\rho \sim r^{-3}$) and rotation curves that peak at ~ 10 AU and then monotonically decline with radius up to $R \sim 100$ AU. Higher resolution would be required to follow the formation and structure of these disks with AMR properly.

The PDF slope $m = -1.67$ at the end of the simulation continues to evolve slowly toward shallower values, but may still remain steeper than -1.5 corresponding to the r^{-2} density profile. Neither does it approach -2 of the EW solution. Interestingly, a similar slope of -1.64 was independently obtained by Collins et al. (2010) in a driven super-Alfvénic AMR MHD turbulence simulation with $M_{\rm s} = 9$. This might indicate that some physics is missing in our discussion above. Indeed, both simulations model self-gravitating supersonic turbulent flows capable of creating the initial conditions for very dynamic collapses involving masses much in excess of the Bonnor–Ebert critical mass (Bonnor 1956; Ebert 1955). Such situations will be better approximated by pressure-free (PF) collapse solutions (Shu 1977). The final stages of self-similar spherically symmetric PF collapse prior to the formation of central singularity are characterized by the $\rho \sim r^{-12/7}$ density profile (Penston 1969) which corresponds to the PDF power-law tail with $m_{\rm PF} = -7/4$. The free-fall collapse approximation, however, always breaks down near the center where the effects of pressure inevitably become important, so the slope of the high end of the PDF should still converge to $m_{\rm LP} = -3/2$. We indeed observe a slope change from -1.7 to -1.5 at $\rho/\rho_0 \approx 10^{6.2}$, see Figure 1. Since the ratio of gravitational-to-pressure forces in the isothermal PF collapse $J^* \propto r^{2/7}$ (Penston 1969), it scales with the mass density as $\rho^{-1/6}$. This weak dependence of J^* on the density is consistent with the appearance of break in slope at very high densities.

The projected density of an infinite sphere with the $\rho \sim r^{-n}$ density distribution,

$$\Sigma(R) = 2\int_0^\infty \rho\left(\sqrt{R^2+x^2}\right)dx \propto R^{1-n}, \qquad (5)$$

also has a power-law PDF,

$$dS \propto d\left(\Sigma^{-\frac{2}{n-1}}\right) \propto d\left(\Sigma^{p}\right), \qquad (6)$$

but with a slope $p = -2/(n-1)$. For the LP, PF, and EW similarity solutions, $p = -2$, -2.8, and -4, respectively.

Figure 3 shows the projected mass density PDFs from the AMR simulation at $t = 0$ (red line) and $t = 0.43t_{\rm ff}$ (blue line). The blue line is based on a subset of the AMR data up to 8 AU in resolution; only the first four levels of fine mesh were used to make the plot. Similar to the three-dimensional density PDF, the initial distribution is well represented by a log-normal. The evolved self-gravitating configuration shows a clear power-law tail at high column densities with a slope of -2.50 ± 0.03. The actual slope uncertainty may be larger than the formally determined value of ±0.03. The distributions in Figure 3 show the average PDFs for all three projections, while only one projection would be available in real observations. The root grid-based high-density tails for individual projections show some bumps (very similar to those seen in Figure 4 of Kainulainen et al. (2009) and some straight sections with slopes broadly varying from as flat as -2 to steeper than -3. Overall, power index $p = -2.5$ measured in the simulation is right in between the predicted slopes for the PF and LP solutions, but the EW option ($p = -4$) seems to be rejected. We expect shallower slopes in simulations with lower Mach numbers or in longer turbulence decay simulations without continuous resupply of kinetic energy from random forcing. Finally, a hint of a shallower slope at $\Sigma > 10^{2.8}$ may indicate the effect of centrifugal support, similar to the slope flattening in Figure 1.

4. DISCUSSION

We do not expect significant differences between driven and decaying turbulence models within the fraction of the first

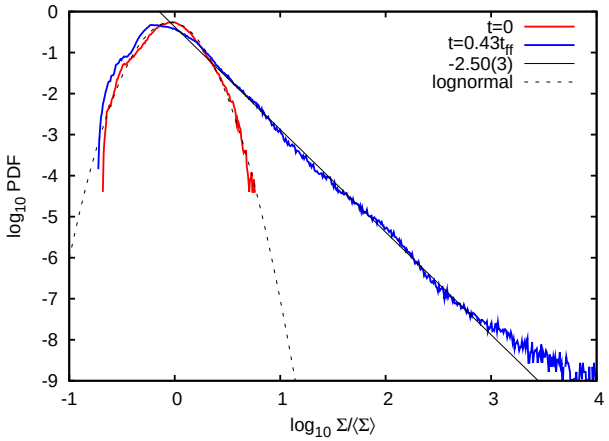

FIG. 3.— Distributions of the projected gas density from the AMR simulation at $t = 0$ (red line) and at $t = 043t_{\rm ff}$ (blue line). The initial distribution has a lognormal shape (dashed line). The final distribution has an extended power-law tail with a slope of -2.50 ± 0.03 (solid line).

free-fall time in this AMR run (see also Offner et al. 2008). By the end of the simulation, the system would still retain $> 70\%$ of the kinetic energy delivered by the stirring force, if self-gravity were not included. However, self-gravity slightly increases the kinetic energy of a turbulent system (e.g., Slyz et al. 2005), thus the lack of forcing does not really make a big difference. Since the free-fall time is shorter than the dynamical time that determines the energy decay timescale, the density PDF established by $t = 0.43t_{\rm ff}$ can be only weakly sensitive to the lack of forcing.

Since the virial parameter for this model is rather small, the role of self-gravity can be somewhat exaggerated. In situations with $\alpha \approx 1$ one should expect a weaker effect. With α close to unity, assuming the same Mach number and domain size, the power-law tail will be shallower (more closely resembling the LP case) in a more extended density range and will depart from the initial lognormal distribution at densities somewhat higher than $\rho/\rho_0 = 10$. While our adopted low value of the virial parameter creates a distribution similar to that of the Taurus molecular cloud, a higher α value would perhaps produce a distribution more similar to that of the Lupus I cloud (see Figure 2 in Kainulainen et al. 2009). Overall, it seems that cloud-to-cloud variations in the virial parameter α and in the age of the cloud in combination with projection effects can account for the full diversity of high-density tails in the observed star-forming clouds (Figure 4 of Kainulainen et al. 2009).

In this discussion on the density PDF, we so far ignored the effects of magnetic fields that are important for star formation. Our recent isothermal and multiphase MHD turbulence calculations, however, both show that variations in the level of magnetization of interstellar clouds make little or no difference for the high-density end of the density PDF (e.g., Kritsuk et al. 2010). In the absence of self-gravity, the high end of the distribution preserves its lognormal shape. In super-Alfvénic turbulence, the magnetic field strength also shows a weak correlation with the gas density of the form $B \sim \rho^{1/2}$ (Padoan & Nordlund 1999; Collins et al. 2010). The most recent Zeeman splitting data for molecular cores also indicate a slope of 0.65 ± 0.05 (Crutcher et al. 2010). A similar relation can be inferred theoretically for dynamically collapsing magnetized protostellar cores (e.g., Scott & Black 1980). Assuming that the correlation $B \sim \rho^{\gamma}$ exists, we predict a similar power-law tail in the PDF of the magnetic field strength with a slope from $-3\frac{1}{2}$ to $-2\frac{1}{4}$ for the range of $\gamma \in [1/2, 2/3]$ and $m \in [-7/4, -3/2]$. A power index of -2.7 measured by Collins et al. (2010) is consistent with $\gamma \approx 0.6$ at $\rho/\rho_0 < 10^3$ and with their PDF slope $m = -1.64$.

5. CONCLUSIONS

We found an intriguing agreement between the probability distribution of molecular cloud densities in recent observations (Kainulainen et al. 2009) and in a deep AMR simulation of self-gravitating, supersonically turbulent molecular cloud (Padoan et al. 2005). In both cases, star-forming clouds display strong deviations from lognormal density distribution in the form of power-law tails at high density. In contrast, clouds with no active star formation display purely lognormal distributions of density.

We attribute the origin of the tails to the fundamental self-similar properties of the r^{-2} isothermal collapse and $r^{-12/7}$ pressure-free collapse laws, which control the density profiles of collapsing structures. This allows us to predict the power-law indices for the mass density ($m \in [-7/4, -3/2]$) and for the projected density ($p \in [-2.8, -2]$) depending on the physical conditions in the parent molecular cloud ($M_{\rm s}$, α, etc.) that broadly agree with both observations and simulation results.

Our results may suggest a reconciliation of various attempts to build a phenomenological theory of star formation and will contribute to the interpretation of numerical simulations in terms of the proposed phenomenologies (e.g., Schmidt et al. 2010; Cho & Kim 2011).

This research was supported in part by a NASA ATP grant NNG056601G, by NSF grants AST-0507768, AST-0607675, and AST-0908740, and by TeraGrid allocations MCA98N020 and MCA07S014. We utilized computing resources provided by the San Diego Supercomputer Center (IBM-P690 *DataStar*, SUN Microsystems *Triton*) and by the National Institute for Computational Sciences (Cray-XT5 *Kraken*).

REFERENCES

Biglari, H., & Diamond, P. H. 1988, Phys. Rev. Lett., 61, 1716
Bonnor, W. B. 1956, MNRAS, 116, 351
Cho, W., & Kim, J. 2011, MNRAS, 410, L8
Collins, D. C., Padoan, P., Norman, M. L., & Xu, H. 2010, ApJ, submitted (arXiv:1008.2402)
Crutcher, R. M., Wandelt, B., Heiles, C., Falgarone, E., & Troland, T. H. 2010, ApJ, 725, 466
Dib, S., & Burkert, A. 2005, ApJ, 630, 238
Ebert, R. 1955, Z. Astrophys., 37, 217
Elmegreen, B. G., & Falgarone, E. 1996, ApJ, 471, 816
Federrath, C., Glover, S. C. O., Klessen, R. S., & Schmidt, W. 2008, Phys. Scr. T, 132, 014025
Hayashi, C., Narita, S., & Miyama, S. M. 1982, Progr. Theor. Phys., 68, 1949
Hennebelle, P., & Chabrier, G. 2008, ApJ, 684, 395
Hunter, C. 1977, ApJ, 218, 834
Kainulainen, J., Beuther, H., Henning, T., & Plume, R. 2009, A&A, 508, L35
Klessen, R. S. 2000, ApJ, 535, 869
Kritsuk, A. G., Norman, M. L., & Padoan, P. 2006, ApJL, 638, L25
Kritsuk, A. G., Norman, M. L., Padoan, P., & Wagner, R. 2007, ApJ, 665, 416
Kritsuk, A. G., Ustyugov, S. D., & Norman, M. L. 2010, arXiv:1011.2177
Krumholz, M. R., & McKee, C. F. 2005, ApJ, 630, 250
Larson, R. B. 1969, MNRAS, 145, 271
Lombardi, M., Lada, C. J., & Alves, J. 2010, A&A, 512, A67

Norman, M. L., Wilson, J. R., & Barton, R. T. 1980, ApJ, 239, 968
Offner, S. S. R., Klein, R. I., & McKee, C. F. 2008, ApJ, 686, 1174
O'Shea, B. W., Bryan, G., Bordner, J., Norman, M. L., Abel, T., Harkness, R., & Kritsuk, A. 2005, in Lecture Notes in Computational Science and Engineering 41, Adaptive Mesh Refinement — Theory and Applications, ed. T. Plewa, T. Linde, & V. G. Weirs (Berlin: Springer), 341
Padoan, P., Kritsuk, A., Norman, M. L., & Nordlund, Å. 2005, ApJ, 622, L61
Padoan, P., & Nordlund, Å. 1999, ApJ, 526, 279
Padoan, P., & Nordlund, Å. 2002, ApJ, 576, 870
Passot, T. & Vázquez-Semadeni, E. 1998, Phys. Rev. E, 58, 4501
Penston, M. V. 1969, MNRAS, 144, 425
Perdang, J. 1990, Vistas Astron., 33, 371
Rosolowsky, E. W., Pineda, J. E., Kauffmann, J., & Goodman, A. A. 2008, ApJ, 679, 1338
Scalo, J., Vázquez-Semadeni, E., Chappell, D., & Passot, T. 1998, ApJ, 504, 835
Schmidt, W., Kern, S. A. W., Federrath, C., & Klessen, R. S. 2010, A&A, 516, A25
Scott, E. H., & Black, D. C. 1980, ApJ, 239, 166
Shu, F. H. 1977, ApJ, 214, 488
Slyz, A. D., Devriendt, J. E. G., Bryan, G., & Silk, J. 2005, MNRAS, 356, 737
Toomre, A. 1982, ApJ, 259, 535
Truelove, J. K., Klein, R. I., McKee, C. F., Holliman, J. H., II, Howell, L. H., & Greenough, J. A. 1997, ApJ, 489, L179
Vázquez-Semadeni, E. 1994, ApJ, 423, 681
Vázquez-Semadeni, E., González, R. F., Ballesteros-Paredes, J., Gazol, A., & Kim, J. 2008, MNRAS, 390, 769
von Weizsäcker, C. F. 1951, ApJ, 114, 165
Whitworth, A. P., Bhattal, A. S., Francis, N., & Watkins, S. J. 1996, MNRAS, 283, 1061
Whitworth, A., & Summers, D. 1985, MNRAS, 214, 1